The 5′ Leader of Precursor tRNA^{Asp} Bound to the *Bacillus subtilis* RNase P Holoenzyme Has an Extended Conformation†

David Rueda,‡,§ John Hsieh,‡ Jeremy J. Day-Storms,|| Carol A. Fierke,*,‡,|| and Nils G. Walter*,‡

Departments of Chemistry and Biological Chemistry, University of Michigan, Ann Arbor, Michigan 48109

Received September 19, 2005

ABSTRACT: RNase P catalyzes the 5′ maturation of transfer RNA (tRNA). RNase P from *Bacillus subtilis* comprises a large RNA component (130 kDa, P RNA) and a small protein subunit (14 kDa, P protein). Although P RNA alone can efficiently catalyze the maturation reaction in vitro, P protein is strictly required under physiological conditions. We have used time-resolved fluorescence resonance energy transfer on a series of donor-labeled substrates and two acceptor-labeled P proteins to determine the conformation of the pre-tRNA 5′ leader relative to the protein in the holoenzyme−pre-tRNA complex. The resulting distance distribution measurements indicate that the leader binds to the holoenzyme in an extended conformation between nucleotides 3 and 7. The conformational mobility of nucleotides 5−8 in the leader is reduced, providing further evidence that these nucleotides interact with the holoenzyme. The increased fluorescence intensity and lifetime of the 5′-fluorescein label of these leaders indicate a more hydrophobic environment, consistent with the notion that such interactions occur with the central cleft of the P protein. Taken together, our data support a model where the P protein binds to the 5′ leader between the fourth and seventh nucleotides upstream of the cleavage site, extending the leader and decreasing its structural dynamics. Thus, P protein acts as a wedge to separate the 5′ from the 3′ terminus of the pre-tRNA and to position the cleavage site in the catalytic core. These results reveal a structural basis for the P protein dependent discrimination between precursor and mature tRNAs.

Both RNA and protein molecules are capable of catalyzing multiple turnover reactions. Yet, these components can also assemble into ribonucleoproteins (RNPs) and, together, enhance catalysis. RNPs vary vastly in size and perform numerous important biological functions. For example, the ribosome catalyzes peptidyl transfer during protein synthesis (*1*), and ribonuclease P (RNase P)[1] catalyzes endonucleolytic removal of the 5′ leader during precursor transfer RNA (pre-tRNA) maturation (*2*−*5*). Because the RNA and protein components work synergistically, their individual roles in catalysis are challenging to distinguish.

RNase P is found in all kingdoms of life (*Archaea*, *Bacteria*, and *Eucarya*) (*2*−*5*). The *Bacillus subtilis* RNase P consists of a large RNA [P RNA, 401 nucleotides (nt), 130 kDa] and a single small protein (P protein, 118 residues, 14 kDa), making it an ideal model system to study the functional and structural synergy between its two components (Figure 1A). High-resolution X-ray crystal structures of RNase P RNA from *Thermotoga maritima* (6) and *Bacillus stearothermophilus (7)* and of RNase P protein from *Thermotoga maritima (8)* and *Bacillus subtilis* are available (*9*), but only structural models have been proposed for the RNase P holoenzyme (*10*). The P RNA subunit alone catalyzes pre-tRNA cleavage in vitro but only in high salt concentrations (*11*), which implies that P RNA harbors most of the active site. The P RNA is constructed in modular parts, with a catalytic domain (C-domain) and a substrate specificity domain (S-domain) (*12*). Multiple contacts between the pre-tRNA substrate and P RNA have been established in biochemical studies (*13*−*19*). For example, the S-domain interacts with 2′-OH groups in the pre-tRNA T-stem and loop and enhances substrate affinity (*13*−*16*). The C-domain, which contains the active site, also forms important contacts to the substrate (*17*−*19*). For example, nucleotides in the J15/16 internal bulge of *Escherichia coli* RNase P RNA form Watson−Crick base pairs with the 3′ RCC of the pre-tRNA RCCA motif (*17*, *18*), and the nt immediately upstream of the cleavage site base pairs with a conserved adenine in J5/15 (*19*). On the basis of the recent crystal structure of RNase P RNA from the thermophilic bacterium *T. maritima*, a model for the interaction with the pre-tRNA substrate in the absence of the P protein has been proposed (*6*).

The P protein subunit is required for RNase P activity under physiological conditions and in vivo (*11*, *20*, *21*). In *B. subtilis* RNase P, the protein component greatly enhances the catalytic efficiency by increasing the binding affinity of

† This work was supported by NIH Grants GM55387 (C.A.F.) and GM62357 (N.G.W.).

* To whom correspondence should be addressed. C.A.F.: phone, (734) 615-2678; fax, (734) 647-4865; e-mail, fierke@umich.edu. N.G.W.: phone, (734) 615-2060; fax, (734) 647-4865; e-mail, nwalter@umich.edu.

‡ Department of Chemistry, University of Michigan.

§ Current address: Department of Chemistry, Wayne State University, 5101 Cass Ave., Detroit, MI 48202.

|| Department of Biological Chemistry, University of Michigan.

[1] Abbreviations: DTT, dithiothreitol; fwhm, full width at half-maximum; GMPS, guanosine 5′-monothiophosphate; 5-IAF, 5-(iodoacetamido)fluorescein; nt, nucleotide(s); pre-tRNA, precursor tRNA; P protein, protein subunit of RNase P; P RNA, RNA subunit of RNase P; RNase P, ribonuclease P; TMR, tetramethylrhodamine; 5-TMRIA, tetramethylrhodamine-5-iodoacetamide; tr-FRET, time-resolved fluorescence resonance energy transfer; tRNA, transfer RNA.

10.1021/bi0519093 CCC: $30.25
Published on Web 11/16/2005

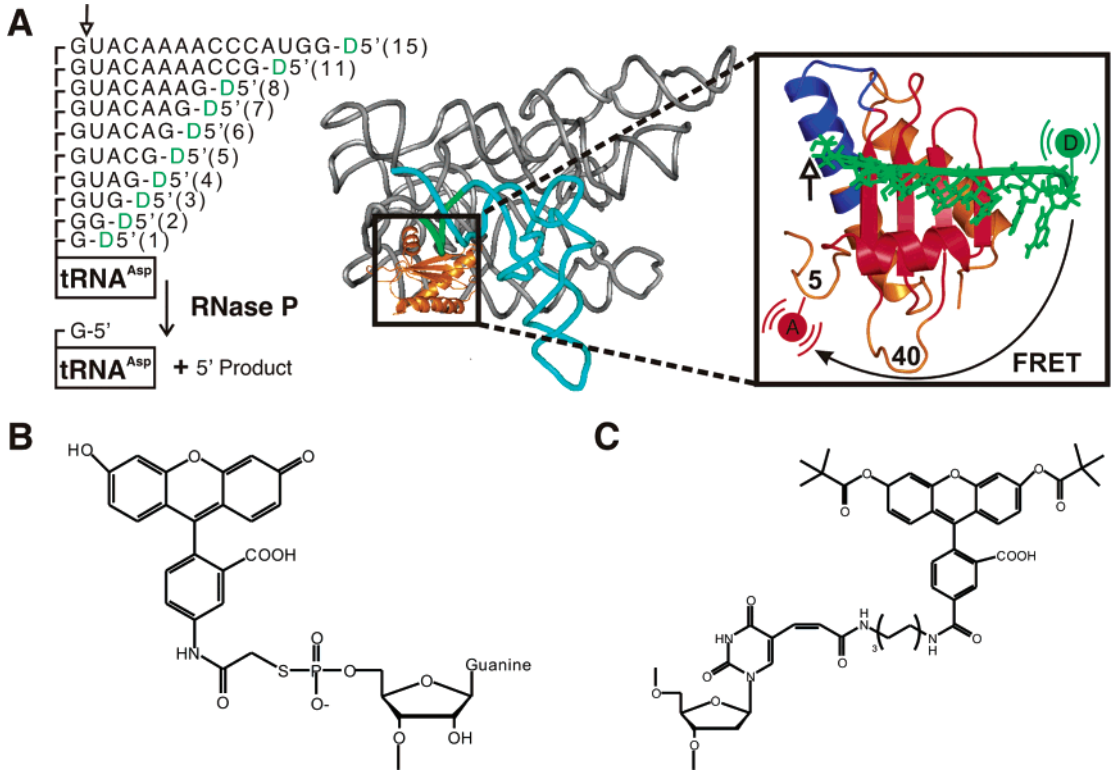

FIGURE 1: The fluorophore-labeled *B. subtilis* RNase P holoenzyme−pre-tRNA^{Asp} complex. (A) Schematic of the RNase P-catalyzed cleavage of pre-tRNA^{Asp} and model for the RNase P−pre-tRNA complex, modified from ref *10*. P RNA is shown in gray, P protein in orange (RNR motif in blue and central cleft in red), and the tRNA^{Asp} in cyan (5′ leader in green, length = 9 nt). The cleavage site is indicated by the hollow arrow. FRET occurs between the donor (D, fluorescein) and acceptor (A, tetramethylrhodamine) fluorophores. The enlarged figure is rotated for image clarity. The donor is attached to a G introduced at the 5′ end of the various pre-tRNA^{Asp} sequences used in this study (left), while the acceptor is coupled to a single cysteine 5 near the protein's N-terminus or a single cysteine 40 on the metal binding loop. Consistent throughout this study, the nt position is obtained as the length of the 5′ leader used in the experiment plus one nt to account for the size of the 5′-fluorescein and its attachment linker. (B) Structure of fluorescein linked to 5′-GMPS as employed for transcription initiation of enzymatically generated 5′ leaders. (C) Structure of fluorescein-dT (Glen Research Corp.) as employed for incorporation into synthetic 5′ leaders.

the holoenzyme for pre-tRNA and for divalent cations in vitro, without significantly affecting the affinity for mature tRNA (the product of the reaction, Figure 1A) (*22*−*24*). The crystal structure of the *B. subtilis* P protein revealed two regions likely to bind RNA: a large central hydrophobic cleft and an unusual left-handed $\beta\alpha\beta$ crossover that contains the highly basic RNR motif (Figure 1) (*9*). Photoaffinity cross-linking studies suggested a direct interaction between the 5′ leader of the pre-tRNA substrate and P protein, locating the active site of the holoenzyme near the protein−RNA interface (*10*, *25*). Biochemical studies have shown that the protein component decreases the concentration of monovalent and divalent cations required for efficient catalysis by RNase P (*11*, *21*). Although divalent cations are required for cleavage, the enzyme−substrate complex can form in their absence (*24*). Taken together, these observations lead to the hypothesis that the protein component of *B.* subtilis RNase P interacts directly with the 5′ leader of the pre-tRNA substrate to increase substrate affinity (*10*, 25), implying an enhanced discrimination between precursor and mature tRNAs (*4*). Yet, the structure of these protein−RNA interactions is not well understood.

To probe the nature of the P protein−pre-tRNA interaction, we have measured the conformation of the 5′ leader relative to the protein in the holoenzyme−substrate complex using time-resolved fluorescence resonance energy transfer (tr-FRET) on 5′-fluorescein-labeled pre-tRNAs containing variable 5′ leader lengths combined with two different tetramethylrhodamine-labeled P proteins. Our distance measurements indicate that the nucleotide segment 3−7 nt upstream of the cleavage site adopts a more extended conformation than a typical single- or double-stranded A-type helix and has reduced flexibility. In addition, fluorescence intensity and lifetime measurements suggest that the local environment of fluorescein when attached to this segment is more hydrophobic. tr-FRET measurements using 10 nt long leaders labeled internally at positions 3, 5, or 7 also support our conclusions. These results are consistent with a model where this 5′ leader segment directly interacts with P protein. Furthermore, our data provide distance constraints that can be used to enhance models of the holoenzyme−substrate complex structure.

MATERIALS AND METHODS

Materials. Chemicals were purchased from commercial suppliers with the highest purity possible. NTP's were purchased from Amersham BioScience (Piscataway, NJ). Plasmids encoding *B. subtilis* pre-tRNA^{Asp} with varying 5′ leader lengths and the K5C and R40C single-cysteine mutants of *B. subtilis* P protein were prepared by Dr. S. Niranjanakumari (*22*, *26*). P protein and P RNA were prepared as previously described (*25*, *26*). Guanosine 5′-monothiophosphate (GMPS, Figure 1B) was synthesized as previously described (*27*). Solutions were degassed prior to use in tr-

FRET measurements. 5-(Iodoacetamido)fluorescein (5-IAF, Figure 1B) and tetramethylrhodamine-5-iodoacetamide (5-TMRIA) were purchased from Molecular Probes (Eugene, OR).

Protein Labeling. Single-cysteine P protein mutants were first incubated with 10 mM dithiothreitol (DTT) in STE buffer (100 mM KCl, 2 mM EDTA, 10% glycerol, and 50 mM Tris-HCl, pH 8.0, at 25 °C) for 30 min at room temperature. Excess DTT was then removed by dialysis at room temperature into STE buffer (four buffer changes, 40 min each). The concentration of the dialyzed protein was determined by absorption at 280 nm [ϵ_{280}(P protein) = 5500 M^{-1} cm^{-1}]. P protein was labeled by incubating a 10-fold molar excess of 5-TMRIA with 100 μM single-cysteine P protein mutant in STE buffer at 4 °C overnight. The reaction was terminated by addition of 10 mM DTT. Excess fluorophore was removed from the labeled P protein by dialysis into STE buffer (three buffer changes, 6 h each). The concentrations of P protein and tetramethylrhodamine (TMR) were calculated from absorption at 280 and 548 nm, respectively, in TE buffer, pH 8.0 [ϵ_{548}(TMR) = 7.8×10^4 M^{-1} cm^{-1} and ϵ_{280}(TMR) = 2.45×10^4 M^{-1} cm^{-1}]. Since both P protein and TMR absorb at 280 nm, the concentration of P protein is calculated as

$$[\text{P protein}] = \left[A(280) - A(548)\frac{\epsilon_{280}(\text{TMR})}{\epsilon_{548}(\text{TMR})}\right]\frac{1}{\epsilon_{280}(\text{P protein})} \quad (1)$$

On the basis of the concentration of P protein and TMR in the purified labeled protein, we conclude that >98% of the P protein is routinely labeled and was therefore used without further purification.

Pre-tRNA^{Asp} Synthesis and Labeling. Precursor tRNA^{Asp} containing a 5′-monothiophosphate was prepared by in vitro transcription using T7 RNA polymerase [prepared using a plasmid kindly provided by W. T. McAllister (*28*)] in the presence of GMPS (4 mM ATP, CTP, UTP, and GMPS, 0.8 mM GTP, 0.1 μg/μL T7 RNA polymerase, 0.1 μg/μL linearized DNA template, 28 mM $MgCl_2$, 1 mM spermidine, 5 mM DTT, and 50 mM Tris-HCl, pH 8.0, incubated at 37 °C for 4 h). Consequently, >80% of pre-tRNA^{Asp} substrates are primed with 5′-GMPS. Transcription reactions were terminated by addition of 30 mM EDTA, and the RNA was concentrated 10-fold and exchanged into TE buffer (10 mM Tris-HCl, pH 7.0, and 2 mM EDTA) by centrifugal filtration (Microcon; Millipore, Billerica, MA). A 10-fold molar excess of 5-IAF dissolved in DMSO was added to the pre-tRNA^{Asp} solution and incubated overnight in the dark at 4 °C. The labeling reaction was terminated by addition of DTT or 2-mercaptoethanol (10 mM). The 5′-fluorescein labeled pre-tRNA^{Asp} was purified by denaturing gel electrophoresis (8% polyacrylamide, 8 M urea) and HPLC as previously described (*29*, *30*).

Fl-pre-tRNA^{Asp} Preparation by Ligation. Chemically synthesized oligoribonucleotides containing a fluorescein were purchased from the W. M. Keck Oligonucleotide Synthesis Facility at Yale University. Sequences: FR3, 5′-UCC UCU UXA UGG UCC-3′; FR5, 5′-UCC UCX UUA UGG UCC-3′; FR7, 5′-UCC XCU UUA UGG UCC-3′; where X is fluorescein-dT (Figure 1C; Glen Research Corp., Sterling, VA). The oligoribonucleotides and a 5′-truncated version of *B. subtilis* tRNA^{Asp} missing five nucleotides at the 5′ end were first annealed to a DNA splint (sequence: 5′-CTG AAC TAC CGG ACC ATA AAG AGG A-3′) and then ligated using T4 DNA ligase (*31*, *32*). Ligation products were purified from starting material by denaturing gel electrophoresis as described above.

Distance Measurements by Time-Resolved FRET. The 5′ leader conformation of pre-tRNA^{Asp} in complex with the *B. subtilis* RNase P holoenzyme was probed by tr-FRET, similarly to previously described procedures (*33*, 34). First, 4 μM P RNA or fluorescein-labeled pre-tRNA (donor) in water was denatured at 95 °C for 2 min and incubated at 37 °C for >15 min. P RNA or pre-tRNA was refolded by dilution into 2× standard buffer (final conditions: 50 mM Tris-HCl, 50 mM MES, pH 6, 20 mM $CaCl_2$, 150 mM KCl, 10 mM imidazole, and 10 mM DTT). Next, the holoenzyme was formed by addition of a stoichiometric amount of either unlabeled or TMR-labeled P protein (2 μM final concentration) to the P RNA, followed by incubation for 30 min at 37 °C (*26*). Finally, the holoenzyme−substrate complex was formed by addition of folded 5′-fluorescein-labeled pre-tRNA^{Asp} of variable leader length (final concentration 1 μM) to the preformed holoenzyme complex and incubated for an additional 15 min at 37 °C. Under these conditions, the cleavage rate constant is less than 0.07 h^{-1} (*23*). The fluorescein emission decay of the donor-only complex was measured and fit to a sum of three exponential decays characterized by their lifetime (τ_i) and relative amplitude (α_i), as previously described (*33*, *34*). Likewise, the doubly labeled holoenzyme−substrate complex was formed using the TMR-labeled K5C or R40C P protein mutants. The fluorescein emission decay in the presence of the acceptor fluorophore, $I_{DA}(t)$, was then measured and fit with the expression:

$$I_{DA}(t) = \int P(R)\sum_i \alpha_i \exp\left(-\frac{t}{\tau_i}\left[1 + \left(\frac{R_0}{R}\right)^6\right]\right) dR \quad (2)$$

where τ_i and α_i are the singly labeled lifetime parameters, R_0 is the Förster distance for 50% energy transfer (55 Å for the fluorescein−TMR pair) (*35*), and $P(R)$ is the distance distribution. The latter was modeled as a three-dimensional weighted Gaussian:

$$P(R) = 4\pi R^2 N \exp[-\sigma(R-\mu)^2] \quad (3)$$

where σ and μ describe the shape of the Gaussian and N is a normalization constant. An additional adjustable parameter was the fraction of singly labeled component (typically 30−45%), caused by unbound fluorescein-labeled pre-tRNA^{Asp}, or photobleached acceptor fluorophore. In the case of the product complex (leader length = 0) this parameter increased up to ~85% due to the fact that the holoenzyme has significantly lower affinity for the mature tRNA^{Asp} (*22*). In our experiments, however, we were able to accurately distinguish the contribution from singly labeled and doubly labeled complexes, as confirmed by deliberately spiking the sample with singly labeled material and still recovering the same distance distribution. An instrument function was systematically measured using a dilute solution of nondairy creamer as scattering solution to deconvolute the fluorescence decays before fitting to the equations above.

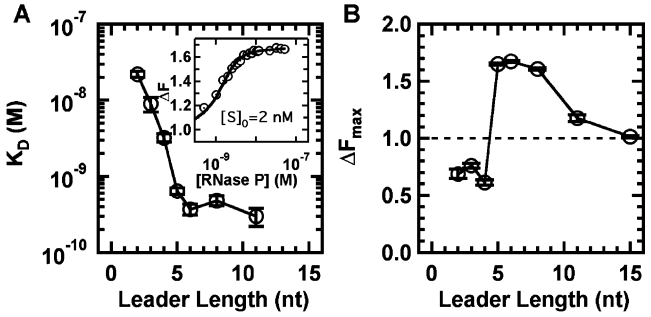

FIGURE 2: Fluorescence titration of fluorescein-labeled pre-tRNA with RNase P holoenzyme. (A) RNase P binding affinity for fluorescein-labeled pre-tRNA as a function of leader length. Binding affinity increases monotonically (i.e., the equilibrium dissociation constant K_D decreases) and then becomes leader length independent. Inset: Fluorescence enhancement of 2 nM substrate (S) Fl-tR5 upon titration with the wild-type RNase P holoenzyme. The line overlaying the data is a least-squares fit of the data to eq 7 (Materials and Methods), yielding an apparent dissociation constant $K_D = 0.35 \pm 0.06$ nM. Error bars arise from at least three independent assays. (B) Fluorescence enhancement (or quenching if $\Delta F_{max} < 1$) of fluorescein-labeled pre-tRNA bound to RNase P as a function of leader length. A fluorescence enhancement of fluorescein indicates that the fluorophore is located in a more hydrophobic local environment.

Anisotropy Measurements. The fluorescence anisotropies of the donor and acceptor fluorophores were measured on a Fusion Universal microplate analyzer (Packard Instrument Co., Meriden, CT) as previously described (*36*). To confirm that the distance distribution measurements observed by tr-FRET were not influenced by large changes in donor or acceptor anisotropy, the holoenzyme−substrate complex was prepared with variable leader length in standard buffer as described above. The *G* factor was determined experimentally using samples with 1 μM free fluorescein or 1 μM free tetramethylrhodamine in standard buffer ($G_F = 0.989$ and $G_{TMR} = 0.919$, respectively). Fluorescein and tetramethylrhodamine were excited at 485 ± 10 and 535 ± 10 nm, respectively, and emissions were collected at 535 ± 12 and 580 ± 12 nm, respectively, with polarized band-pass filters. Each measurement was repeated 10 times, and the standard deviations were less than 1%.

Pre-tRNA Binding Affinity by Fluorescence Titration. Fluorescence titrations were performed by titration of unlabeled wild-type *B. subtilis* RNase P holoenzyme (0.5 nM to 10 μM) into 1, 2, or 3 nM fluorescein-labeled pre-tRNA^{Asp} (Figure 2), under the same solution conditions as those of the tr-FRET experiments (50 mM Tris-HCl, 50 mM MES, pH 6.0, 20 mM $CaCl_2$, 150 mM KCl, and 20 mM DTT at 25 °C). Fluorescein was excited at 488 ± 8 nm, and its emission was measured at 524 ± 10 nm after each holoenzyme addition using a fluorometer (Aminco-Bowman Series 2; Thermo Electron Corp., Houston, TX). The fluorescence enhancement, ΔF, was calculated as (*37*)

$$\Delta F = \frac{(F_{final} - F_{blank})}{F_{initial}} \frac{V_{final}}{V_{initial}} \quad (4)$$

where $F_{initial}$ and F_{final} are the initial and final fluorescence intensities, respectively, and $V_{initial}$ and V_{final} are the corresponding solution volumes to correct for volume increases. F_{blank} is the fluorescence intensity change in a blank control titration without fluorescent pre-tRNA. When the value of $\Delta F < 1$, then fluorescence quenching occurs instead of enhancement. Fluorescein-labeled pre-tRNA^{Asp} substrate binding to RNase P holoenzyme can be described by a 1:1 (stoichiometric) binding equilibrium (*22*)

$$E + S \rightleftharpoons ES \quad (5)$$

where E is the free RNase P holoenzyme, S is the fluorescein-labeled pre-tRNA^{Asp}, and ES is the holoenzyme−pre-tRNA complex. Please note that in the high salt concentrations in the assay the RNase P holoenzyme remains as a monomer (*38*, *39*). The dissociation constant, K_D, is defined as

$$K_D = [E][S]/[ES] \quad (6)$$

The observed relative fluorescence enhancement ΔF as a function of enzyme concentration was fit with the binding isotherm:

$$\Delta F = \Delta F_0 + (\Delta F_{max} - \Delta F_0)\{((K_D + [E]_0 + [S]_0) - \sqrt{(K_D + [E]_0 + [S]_0)^2 - 4[E]_0[S]_0})/2[S]_0\} \quad (7)$$

where ΔF is the observed fluorescein fluorescence enhancement (or quenching) and $[E]_0$ and $[S]_0$ are the initial enzyme and substrate concentrations, respectively. ΔF_0 and ΔF_{max} are the fluorescence enhancement in the absence of enzyme and at saturation, respectively. For each leader length fluorescence titrations were performed at $[S]_0 = 1$, 2, and 3 nM. In our fits, $[S]_0$ was held constant at its corresponding value (1, 2, or 3 nM), and ΔF_0 was held constant at 1.

Building a Model of the Holoenzyme−Substrate Complex. We built a model of the 5′ leader RNA backbone trajectory using the software package PyMOL (www.pymol.org) (*40*). We first loaded the existing model of the holoenzyme−substrate complex by Westhof, Gopalan, and co-workers (*10*). Then, we used the editing tools built in PyMOL to manually move the backbone 5′-phosphates. The distance between the 5′-phosphates in the leader and the αC of K5 and R40 was determined using the measurement wizard in PyMOL, and subsequently the positions of the backbone 5′-phosphate were manually moved until the measured distances were within 1 Å of the experimentally observed ones (panels A and B of Figure 3, respectively). A backbone trajectory was drawn between the resulting 5′-phosphate positions (Figure 5).

RESULTS

Fluorophore Labels on the Pre-tRNA Do Not Affect Binding to RNase P Holoenzyme. The binding affinities of pre-tRNA^{Asp} variants with various 5′ leader lengths to *B. subtilis* RNase P holoenzyme have been previously characterized using a gel filtration technique (*22*). These experiments showed that the substrate binding affinity increases with the 5′ leader length, indicating the presence of interactions between the substrate and the holoenzyme. To test whether introduction of a terminal fluorophore label on the 5′ leader affects substrate binding affinity by the holoenzyme, we labeled the 5′ end of various pre-tRNA^{Asp} substrates (consistently containing a 5′ G) with fluorescein and measured the dissociation constant of the enzyme−substrate complex using fluorescence titrations (*37*, *41*). Please note that, to adjust for the extension that our fluorescein probe

imposes on the 5′ leader, one nt is consistently added to the count of nucleotides upstream of the cleavage site (Figure 1A). The inset in Figure 2A shows a typical fluorescence titration, in which the fluorescence enhancement (ΔF, eq 4) of a 6 nt long labeled substrate ($[S]_0 = 2$ nM) is measured at increasing holoenzyme concentrations. A simple stoichiometric binding isotherm (eq 7) is fit to these data to obtain the binding affinity ($K_D = 0.35 \pm 0.06$ nM) and the fluorescence enhancement at saturation ($\Delta F_{max} = 1.7 \pm 0.1$, indicating an overall 70% increase in fluorescence intensity). Three titrations at different substrate concentrations ($[S]_0 =$ 1, 2, and 3 nM) were used to determine the corresponding dissociation constant unambiguously. Figure 2A shows the dependence of K_D on the 5′ leader length. The pre-tRNA dissociation constant from the RNase P−holoenzyme complex decreases from 22 ± 2 nM for fluorescein-labeled $tRNA^{Asp}$ (1 nt long) to 0.3 ± 0.1 nM for labeled pre-tRNA with 5′ leaders of ≥5 nt. These results are consistent with the binding affinities of nonlabeled pre-tRNAs, as previously determined by gel filtration (*22*, *23*). This indicates that the attachment of a 5′ fluorophore to the leader does not have a significant effect on the binding interactions between the RNase P holoenzyme and its substrates.

The fluorescein enhancement at saturation is also dependent on the length of the 5′ leader length (Figure 2B). 5′ leaders shorter than 5 nt exhibit fluorescence quenching ($\Delta F_{max} < 0.7$), while 5′ leaders 5− 8 nt long exhibit significant fluorescence enhancement ($\Delta F_{max} > 1.5$). This fluorescence enhancement decreases and finally disappears for 5′ leaders 11 and 15 nt long (Figure 2B). It has long been known that the relative steady-state fluorescence intensity of a fluorophore reports on its local environment (*41*, *42*). The fluorescence enhancement observed for 5′ leaders 5−8 nt in length therefore suggests that the fluorescein label is exposed to a hydrophobic environment, such as the central cleft of the P protein, which is rich in aromatic amino acid side chains (*9*). As the leader length increases beyond 8 nt, the 5′-fluorescein emerges from this hydrophobic environment, and therefore the fluorescence intensity becomes comparable to that of the free pre-tRNA ($\Delta F_{max} \approx$ 1.0). Stacking interactions with neighboring bases in either the 5′ leader or P RNA (see Figure 1A) may result in the fluorescence quenching observed with 5′ leaders shorter than 5 nt.

Distance Measurements Suggest That nt 4−7 of the Pre-tRNA 5′ Leader Adopt an Extended Conformation. Interactions between the RNase P holoenzyme and pre-$tRNA^{Asp}$ with 5′ leaders longer than 4 nt have increased binding affinity (Figure 2A), which gives rise to enhanced discrimination between the substrate and the product of the maturation reaction. To further probe the nature of these interactions, we measured the conformation of the 5′ leader relative to the P protein using tr-FRET. For this purpose, we used our various 5′-fluorescein-labeled pre-$tRNA^{Asp}$ substrates as FRET donor and paired them with a tetramethylrhodamine (TMR) labeled K5C single-cysteine mutant of the P protein as FRET acceptor (see Materials and Methods, Figure 1A). The K5C mutation is located near the accessible N terminus of the P protein and neither affects catalytic activity nor substrate binding (data not shown). We then measured a series of donor−acceptor distance distributions for pre-tRNAs containing a 5′ leader of 1 (product tRNA plus

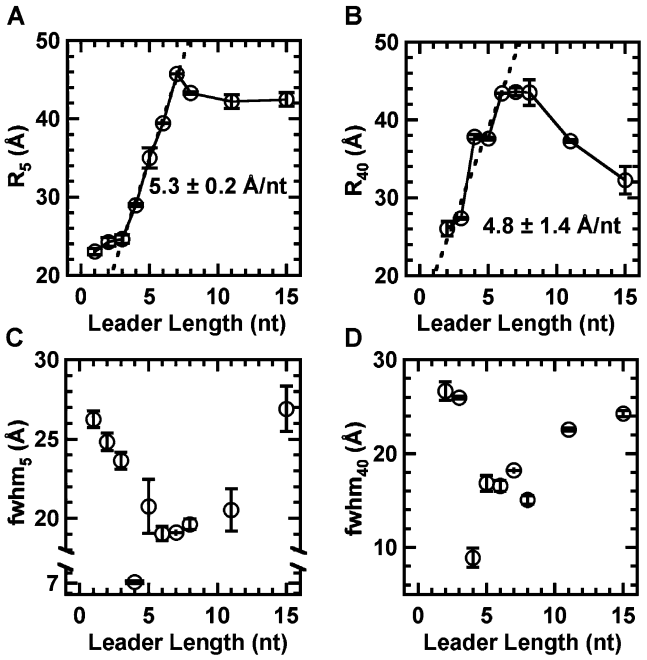

FIGURE 3: Time-resolved FRET experiments on the *B. subtilis* RNase P holoenzyme−pre-$tRNA^{Asp}$ complex. Upper panels: Mean donor−acceptor distance for the rhodamine-labeled K5C (A) and R40C (B) mutants as a function of 5′ leader length (50 mM Tris-HCl−MES, pH 6.0, 20 mM $CaCl_2$, 150 mM KCl, 10 mM imidazole, and 10 mM DTT at 25 °C). The dashed lines yield the indicated slopes for leaders between 3 and 7 nt and between 2 and 6 nt in length, respectively. Lower panels: Full width at half-maximum (fwhm) for the rhodamine-labeled K5C (C) and R40C (D) mutants as a function of 5′ leader length. Error bars arise from two independent assays.

fluorophore), 2, 3, 4, 5, 6, 7, 8, 11, and 15 nt in the presence of 20 mM Ca^{2+} and at pH 6, conditions where catalysis of pre-tRNA cleavage is slow (≤0.07 h^{-1}) (*23*). Each distance distribution is characterized by a mean distance between the fluorophores (R_5, Figure 3A) and a full width at half-maximum ($fwhm_5$, Figure 3C). The mean distance between donor and acceptor fluorophore in the product complex is ∼23 Å (Figure 3A). This distance increases linearly with a slope of 5.3 ± 0.2 Å/nt for leader lengths between 3 and 7 nt (dashed line, Figure 3A), suggesting that the leader has a well-defined, regular conformation as it extends across the holoenzyme. For comparison, the average length of denatured single-stranded RNA is 2.1−2.5 Å/nt (*43*), while the axial rise per nt in an RNA duplex varies between 2.8 and 3.1 Å/nt (*44*). These values are substantially shorter than the 5.3 Å/nt slope observed here, suggesting that the conformation of the single-stranded 5′ leader is rather extended (Figure 1A). However, this slope is still shorter than the average persistence length of poly(U) (8 Å/nt) measured in optical tweezer pulling experiments in 500 mM Na^+ (*45*). Notably, the ∼21 Å distance increase between the 3 and the 7 nt long 5′ leaders approximately coincides with the 16−20 Å width of the central cleft in the P protein (*9*).

The average donor−acceptor distance for 5′ leader lengths ≥7 nt plateaus around 42 Å (Figure 2A), indicating a distinct conformation of the leader sequence beyond ∼7 nt. Thus, these results suggest that the 5′ leader adopts an extended conformation specifically in the segment between nt 4 and 7 upstream of the cleavage site. This conformation is likely determined by specific interactions with the P protein, as

suggested by our previous kinetic and cross-linking data (*25*).

An additional set of distance measurements was obtained using a second TMR-labeled single-cysteine mutant, R40C. This mutation locates the acceptor fluorophore in the metal binding loop (Figure 1A) (*9*). The resulting average donor−acceptor distances (R_{40}) are shown in Figure 2B. Similarly to the K5C mutant data in Figure 3A, the distance between donor and acceptor first increases for 5′ leaders ≤6 nt and then plateaus between leader lengths of 6 to 8 nt. Beyond 8 nt the distance decreases monotonically, consistent with a distinct conformation of the leader sequence beyond 8 nt as noted above. A linear fit to the initial rise between leader lengths of 3−6 nt yields a slope of 4.8 ± 1.4 Å/nt, very similar to the value observed with the K5C mutant (5.3 ± 0.2 Å/nt; compare dashed lines in panels A and B of Figure 3). The overall ∼18 Å increase measured for the 3−7 nt 5′ leaders using the R40C mutant also closely matches the width of the central cleft of the P protein. A linear fit to the distance decrease between leader lengths of 8−15 nt results in a decrease of only 1.6 ± 0.2 Å/nt slope (not shown), further supporting the notion that the 5′ leader conformations below and above nt 8 are very different.

The Distance Distribution Widths Reveal That the Flexibility of the Pre-tRNA^{Asp} 5′ Leader between nt 5−8 Is Reduced When Bound to the Holoenzyme. Panels C and D of Figure 3 show the fwhm's of the distance distributions measured as a function of leader length for the acceptor-labeled P protein mutants K5C and R40C, respectively. These fwhm's arise from a composite of (i) the intrinsic structural dynamics between the labeled 5′ leader and the labeled P protein and (ii) the mobility of the fluorophores at the end of their attachment linkers (*33*, *34*). In our direct comparison of different 5′ leader lengths, the fluorophores and their attachment linkers are identical for all leaders. Thus, leader length dependent variations in fwhm can only originate from differences in structural dynamics of the leaders or from changes that result in different structural dynamics between the leaders and the P protein. With the labeled K5C mutant, the observed distance distribution $fwhm_5$ shows a near-parabolic dependence on 5′ leader length (Figure 3C). In the product complex (length = 1) $fwhm_5 = 26.2 \pm 0.5$ Å, which then decreases to ∼18 Å for leaders of 5−8 nt and finally increases for longer leaders. The only outlier from this trend is the 3 nt leader with a substantially lower fwhm of ∼7 Å (see below for further discussion). The decrease in fwhm for the 5−8 nt long leaders is consistent with the idea that this segment of the pre-tRNA^{Asp} 5′ leader interacts with the holoenzyme in a way that limits the structural dynamics. Further extension of the leader results in increased structural dynamics as would be expected for the introduction of a more mobile conformation into the leader beyond a length of 8 nt, where the fluorescein no longer interacts with the holoenzyme.

The observed distance distribution widths with the R40C mutant ($fwhm_{40}$) show a similar near-parabolic dependence on 5′ leader length (Figure 3D). In the one nucleotide long 5′ leader, $fwhm_{40} = 23.7 \pm 2.0$ Å, which decreases to 16.5 ± 0.1 Å for the 6 nt long leader and then finally increases for longer leaders. These results further support the idea that the structural dynamics of the 5′ leader between nt 5 and nt 8 are limited by interactions with the holoenzyme. Alternatively, the holoenzyme may undergo a specific conformational change upon binding substrates 5−8 nt long, thereby conformationally constraining the acceptor rather than the donor fluorophore. This possibility, however, is less favored by the data because the acceptor label at distinct positions (K5C in the N terminus and R40C in the metal binding loop; see Figure 1A) shows similar decreases in flexibility for these specific substrates. In any case, our results provide further evidence for a model where the P protein and the 5′ leader interact between nt 5 and nt 8.

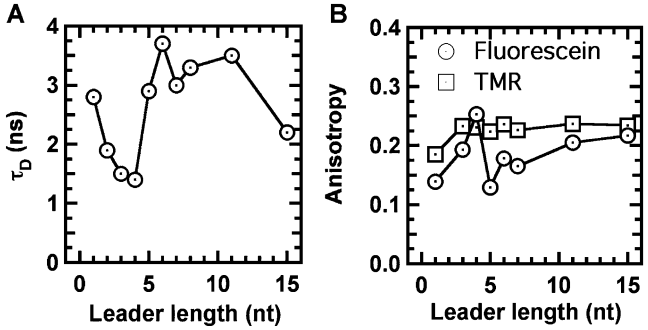

FIGURE 4: Fluorescence properties of the 5′-fluorescein on the pre-tRNA^{Asp} substrate and the TMR on the P protein. (A) Average fluorescein fluorescence lifetime as a function of 5′ leader length. (B) Fluorescein (circles) and TMR (squares) anisotropies as a function of 5′ leader length. Errors from two independent assays are <5%.

Fluorescence Lifetime Measurements Corroborate That nt 5−11 of the 5′ Leader Are Surrounded by a Hydrophobic Environment. Our fluorescence titration data and the width of the measured donor−acceptor distance distributions indicate that the local environment of the 5′-fluorescein changes for leaders 5−8 nt long. In addition, we observe enhanced fluorescence intensity for 5′ leaders 5−8 nt in length. To probe these changes more directly, we measured the average fluorescein fluorescence lifetime in the absence of a FRET acceptor (Figure 4A) (*33*, *37*). In the vicinity of nucleic acid bases, fluorescein fluorescence can be quenched by collisional encounters with nearby guanines, and as a result, its fluorescence lifetime decreases (*33*, *46*). In a hydrophobic environment, however, fluorescence is enhanced, and the fluorescence lifetime increases (*37*). If the segment between nt 5 and nt 8 of the pre-tRNA^{Asp} leader indeed interacts with the central cleft of the P protein in the holoenzyme−substrate complex, then the fluorescence lifetime of the 5′-fluorescein is expected to increase at those leader lengths because of the hydrophobic environment provided by the protein. Figure 4A shows the average fluorescein fluorescence lifetime as a function of leader length. In the product complex (length = 1), the average lifetime is 2.8 ± 0.1 ns. As the leader length increases, the observed average fluorescence lifetime decreases below 2 ns and reaches a minimum (1.4 ± 0.1 ns) at the 4 nt leader length. These very short lifetimes clearly indicate that the fluorescein is strongly quenched, in agreement with the corresponding low fluorescence amplitude observed in Figure 1B ($\Delta F_{max} < 1$). Beyond leader length 4, the average fluorescence lifetime increases dramatically and reaches a maximum for a 6 nt long leader (3.7 ± 0.1 ns). For 5′ leaders 5−11 nt in length, the fluorescein fluorescence lifetime remains approximately constant (3−4 ns) until it finally decreases to 2.2 ± 0.1 ns for the longest leader (15 nt), also in good agreement with the steady-state fluorescence inten-

sity titration (Figure 2B). The average fluorescence lifetime for the product is higher than that of the leaders 2−4 nt in length, possibly because the product has only limited binding affinity to the holoenzyme (Figure 2A), and thus, we are averaging over bound and unbound product. This is not the case for longer leaders because they bind the enzyme with higher affinity (Figure 2A).

These results show that the 5′-fluorescein of leaders 5−11 nt long is located in (or near) a hydrophobic environment, where the collisional encounters between fluorescein and nearby guanosines are limited. As previously suggested (*25*), such an environment may be the hydrophobic central cleft of the P protein. The average fluorescence lifetime for the 4 nt long 5′ leader is shortest, possibly caused by enhanced interactions with guanines of the P RNA or with the 5′-G of the leader (see below for further discussion).

In agreement with the steady-state fluorescence titration measurements (compare Figures 2B and 4A), these data further support our conclusion that the 5′ leader segment 5−8 nt upstream of the cleavage site interacts with the central cleft of the P protein, thus keeping the leader in an extended conformation.

Fluorescein Anisotropies Are Largely Uniform Except for the 3 nt Leader. To confirm that the distance distribution measurements observed by tr-FRET are not significantly influenced by changes in donor or acceptor anisotropy, we measured the fluorescence anisotropies of the donor and acceptor fluorophores as a function of leader length (see Materials and Methods and Figure 4B). In general, both anisotropies are typical values for fluorophores coupled to nucleic acids and vary only slightly with leader length. This finding indicates that the observed changes in fwhm as a function of leader length (Figure 3C,D) do not arise from local changes in fluorophore mobility but rather from changes in 5′ leader dynamics, supporting our conclusions. The fluorescein anisotropy increases substantially for the 4 nt leader, indicating decreased fluorophore mobility at this position. This result suggests that the unusually low fwhm, fluorescence lifetime and ΔF_{max} observed only for this leader (Figures 3C,D, 4A, and 1B, respectively) may arise as a consequence of particularly stable stacking interactions with neighboring guanosines of the P RNA or the leader 5′-G.

Distance Measurements with a 5′ Leader of Fixed Length and Labeled at Variable Internal Positions Confirm Our Conclusions. We sought to test whether the extended 5′ leader conformation in the holoenzyme−substrate complex arises (in part) from the use of 5′ leaders of different lengths or if it is a general property of leaders of any length. For this purpose we prepared, by ligation, three 10 nt long 5′ leaders labeled internally with a fluorescein-2′deoxy-T at positions 3, 5, and 7 (FR3, FR5, and FR7, respectively; see Materials and Methods). The resulting average distances to the acceptor on the P protein mutant K5C were 37.5, 43.8, and 44.5 Å, respectively. Because the fluorophore linkers used here are longer than those used above (compare panels B and C of Figure 1), we observe slightly longer distances, as expected. However, we still observe the same qualitative 5′ leader length dependence as in Figure 3A: the average donor−acceptor distance first increases 6.3 Å between FR3 and FR5 (slope = 3.15 Å/nt) and then saturates between FR5 and FR7 (only 0.7 Å additional increase). These results show that the observed 5′ leader conformations using leaders of variable (Figure 3) and fixed length are comparable. The observed differences in slope are likely due to our limited data set with fixed leader length.

Finally, the widths of the distance distributions measured using FR3, FR5, and FR7 are 24.5, 19.7, and 26.7 Å, respectively. Thus, we observe the same qualitative 5′ leader length dependence of fwhm as in Figure 3C,D, where the fwhm first decreases and then increases with increasing leader length. This result confirms that the reduced flexibility of leaders 5−8 nt in length is also observed when the leader length is held constant, in further support of our model wherein this 5′ leader segment interacts with the central cleft of the P protein.

DISCUSSION

RNase P is an essential riboendonuclease in *Archaea*, *Bacteria*, and *Eucarya* that plays an important role in the maturation pathway of tRNAs, where it cleaves the 5′ leader of precursor tRNAs. It has been previously shown that, in high Mg^{2+} concentrations in vitro, the P RNA component is sufficient for catalysis (*47*). Under physiological conditions in vitro and in vivo, however, the P protein becomes indispensable. Yet, the exact structural and functional role of the protein is not well understood. Previous studies have proposed multiple roles for P protein (for reviews see refs *3*−*5*): (i) P protein decreases the monovalent and divalent cation concentration required for efficient catalysis in vitro (*21*, *47*). (ii) P protein enhances the binding affinity of pre-tRNAs with a 5′ leader longer than 5 nt to the holoenzyme and, thus, increases discrimination over product binding (an inhibitor of the maturation reaction) (*9*, *22*, *23*). Coincidentally, P protein also increases the binding affinity of metal ions that stabilize pre-tRNA binding and enhance catalysis (*24*). (iii) Cross-linking studies have suggested that the central cleft of the P protein interacts with pre-tRNA 5′ leaders at least 4 nt in length, which locates the protein in close proximity to the active site (*25*). (iv) The P protein may alter the structure of the P RNA component (*11*, *48*−*50*). Overall, there is a wealth of biochemical data that positions the highly conserved RNR motif of the P protein near the active site of the RNA enzyme (Figure 1A), in support of a role of the protein in contacting the substrate leader and enhancing binding and catalysis (*9*, *10*, *12*, *51*−*55*).

In an effort to further understand the role of P protein, we have characterized the 5′ leader conformation of pre-$tRNA^{Asp}$ relative to the P protein using fluorescence titrations and tr-FRET. For this purpose we have generated a systematic series of pre-$tRNA^{Asp}$ variants labeled with fluorescein at the 5′ end as FRET donor and two single-cysteine protein mutants, K5C and R40C, labeled with TMR as FRET acceptors in positions 5 and 40, respectively. Our data show that the fluorescein label does not affect pre-tRNA binding to the holoenzyme (Figure 2A), enabling us to use these substrates to study the unperturbed 5′ leader conformation of pre-$tRNA^{Asp}$ bound to the holoenzyme. The observed tr-FRET distance distributions show that both conformation and structural dynamics depend on the position within the 5′ leader (Figure 3). The 5′ leader segment from nt 4 to nt 7 upstream of the cleavage site (Figure 3A,B) adopts an extended conformation, with a distance increase of ∼5.3 Å between each nt. Coincidentally, the structural dynamics of

the 5′ leader segment between nt 5 and nt 8 appear more restricted (Figure 3C,D). Further increases in leader length result in small changes in donor-to-acceptor distance but recover increased structural dynamics. Moreover, the local environment of the terminal fluorescein appears to be more hydrophobic for the 5′ leader segment between 5 and 8 nt upstream of the cleavage site (Figures 2B and 4A).

Taken together, these observations suggest that the 5′ leader is subject to three different local environments from the cleavage site to the furthest 5′ end: (i) The 5′ leader segment up to and including nt 3 upstream of the cleavage site approaches the central cleft of the P protein in a relatively compact conformation (Figure 4A,B) within a comparatively hydrophilic medium (Figures 2B and 4A). (ii) Between nt 4 and nt 7, the 5′ leader lies within the hydrophobic central cleft of the P protein in an extended conformation. This conformation is likely the result of interactions between the substrate and the holoenzyme, which result in decreased structural dynamics (Figure 3C,D) and increased fluorescein fluorescence lifetime and intensity (Figures 2B and 4A). (iii) Beyond nt 7, the 5′ leader exits the protein, contacting a more hydrophilic environment, such as the solvent (Figures 2B and 4A), and adopting a less extended and more dynamic conformation, possibly a random coil (Figure 3C,D).

Additional evidence for this model arises from the following consideration. The hydrophobic cleft in the P protein, ~20 Å across and ~10 Å wide, is formed between an α helix and the face of the central β sheet (Figure 1A) (*9*). Therefore, the overall distances of 21 and 18 Å measured by tr-FRET between nt 3 and nt 7 (panels A and B of Figure 3, respectively) match the dimensions of the central cleft of the P protein in the crystal structure. The three exposed aromatic residues on the α helix [Phe16 and Phe20, which are highly conserved among bacteria (*51*)] and on β strand 2 (Tyr34) are plausible candidates to play a role in the interactions between the P protein and the 5′ leader (Figure 5C) (*9*). In analogy, spliceosomal protein U1A has similar dimensions to the P protein, and its exposed aromatic residues are known to stack with several nucleotides of a bound single-stranded RNA (*56*). Similar stacking interactions between aromatic amino acids and the bases have been observed in other RNA−protein interactions (*57*).

Figure 5 compares our distance measurements to those derived from the structural model developed for the *B. subtilis* holoenzyme−pre-tRNA complex by Westhof, Gopalan, and co-workers (*10*). In this model we measured the distances between the αC of amino acids 5 and 40, respectively, and the 5′-phosphate of each nucleotide in the leader using the software package PyMOL [www.pymol.org (*40*)]. Using this approach we find that the structural model of Westhof and Gopalan is generally in good agreement with our experimental distance measurements; the average phosphate-to-phosphate distance between nt 4 and nt 9 in the structural model is 5.8 Å/nt, very similar to the dimensions we measured by tr-FRET between nt 3 and nt 7 (5.3 ± 0.2 and 4.8 ± 1.4 Å/nt, respectively; Figure 5A,B). (Please note that these slopes represent a lower limit for the absolute distances between nucleotide phosphates because the orientation of the 5′ leader RNA is not necessarily collinear with the vector defined by the two fluorophore locations.) A closer inspection of Figure 5A,B, however, reveals two important differences between the model and our measurements that

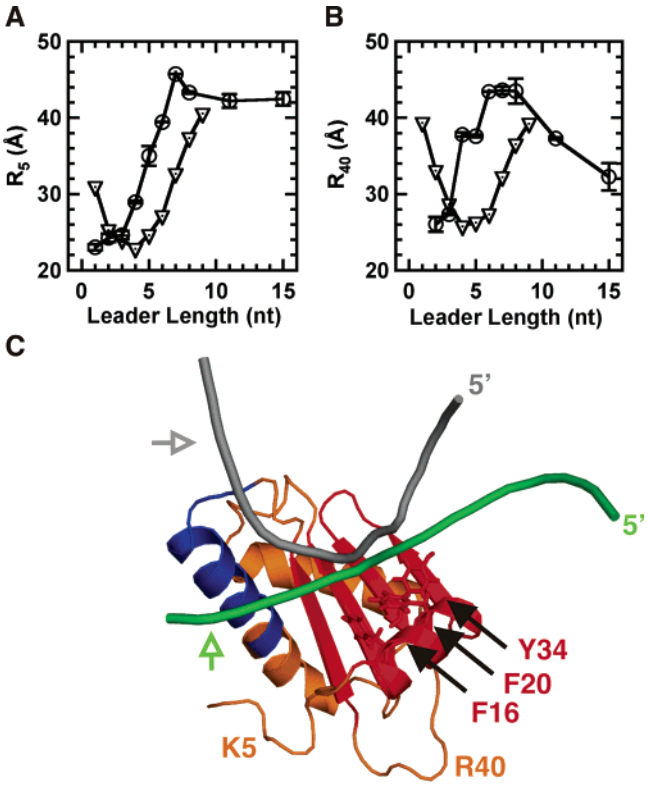

FIGURE 5: Comparison of our experimentally determined distances (circles) for the K5C (A) and R40C (B) mutants of P protein (see also Figure 3A,B) with those predicted by a previously published model (*10*). The distances in the structural model were measured between the αC of amino acids 5 and 40, respectively, and the phosphate of the corresponding nt in the model. (C) Two structural models of the pre-tRNA 5′ leader backbone trajectory (gray, Westhof and Gopalan model; green, refined model from the present study) relative to the P protein (orange; RNR motif in blue and central cleft in red). The cleavage sites are indicated by hollow arrows. The hydrophobic amino acids in the central cleft (F16, F20, and Y36), which possibly interact with the leader, are drawn in stick representation. The single-cysteine mutation sites (K5 and R40) are indicated. The green ribbon depicts the modeled backbone trajectory of the 5′ leader based on the tr-FRET-derived distances of the present study (Materials and Methods). The refined model positions the cleavage site ~2 nt closer to the N terminus of the protein than the Westhof and Gopalan model, while we find the 5′ end of the leader closer to R40. The 5′ leader therefore wraps around the accessible surface of the α helix in the RNR motif of the P protein.

are likely relevant for catalysis. First, our data show that the extended region of the 5′ leader is approximately 2 nt closer to the pre-tRNA cleavage site than in the model (Figure 5A,B). Second, the structural model locates the cleavage site near the N terminus of the highly conserved RNR motif of the P protein (amino acids in blue, Figure 5C). By contrast, building a new model for the P protein−5′ leader interaction based on our tr-FRET measurements (see Materials and Methods) positions the cleavage site near the accessible surface of the α helix in the RNR motif (Figure 5C). Thus, we propose that the 5′ leader wraps around this region of the protein as indicated by the gray ribbon in Figure 5C. Consequently, the protein acts as a wedge to separate the 5′ and 3′ termini of the pre-tRNA, to position the cleavage site in the catalytic core, and to dynamically restrain the 5′ leader. Nonetheless, the protein only enhances the rate of catalysis by a factor of 3 at saturating concentrations of substrate and magnesium (*23*), and therefore it does not participate directly

in catalysis. This model is in agreement with previous experiments using single-cysteine mutants of the P protein derivatized with a copper phenanthroline cleavage reagent, which located the RNR motif of the P protein near the cleavage site and the 3′ terminus of the pre-tRNA (*58*).

In conclusion, the data presented here are consistent with a previously proposed model where the cleavage site of pre-tRNA is located near the protein−P RNA interface (*10*, *25*) and the leader binds to the central cleft of the P protein between nt 3 and nt 7 upstream of the cleavage site (Figure 1) (*10*, *25*). RNase P holoenzyme and pre-tRNA interactions result in an unusually extended conformation with reduced dynamics in this region of the 5′ leader. One may call this the "rack model" of the RNase P−pre-tRNA interaction, after the medieval torture device. Our model supports multiple roles for the P protein: (i) selectively increasing the affinity of the holoenzyme for its pre-tRNA substrate (with leaders >5 nt) by a factor of 10^4 compared to P RNA alone, combined with an only modest increase of the affinity for mature tRNA (*23*) (this leads to an increased discrimination between substrate and product of the reaction); (ii) decreasing the concentration of magnesium required for optimal activity (*24*); (iii) entropically disfavoring the reversal of cleavage (i.e., ligation of a single-stranded RNA to a mature tRNA), as a consequence of the unusually extended conformation of the 5′ leader; (iv) driving a wedge between the 5′ and 3′ termini of the pre-tRNA, fastening the 5′ leader and positioning the cleavage site in the catalytic core of the P RNA. In the absence of the P protein, higher ionic strength can compensate for the loss of these interactions (*24*). Future tr-FRET measurements with the acceptor fluorophore coupled to other residues of the P protein will provide additional distance constraints so as to accurately model the three-dimensional architecture of the RNase P holoenzyme−substrate complex by triangulation.

ACKNOWLEDGMENT

We thank S. Niranjanakumari for the synthesis and purification of single-cysteine mutants of the P protein and Robert Kennedy and his group for kind assistance with the fluorescence anisotropy measurements, as well as current and former members of the Engelke, Fierke, and Walter groups for useful comments and suggestions.

REFERENCES

1. Ramakrishnan, V. (2002) Ribosome structure and the mechanism of translation, *Cell 108*, 557−572.
2. Frank, D. N., and Pace, N. R. (1998) Ribonuclease P: unity and diversity in a tRNA processing ribozyme, *Annu. Rev. Biochem. 67*, 153−180.
3. Kurz, J. C., and Fierke, C. A. (2000) Ribonuclease P: a ribonucleoprotein enzyme, *Curr. Opin. Chem. Biol. 4*, 553−558.
4. Hsieh, J., Andrews, A. J., and Fierke, C. A. (2004) Roles of protein subunits in RNA-protein complexes: lessons from ribonuclease P, *Biopolymers 73*, 79−89.
5. Harris, M. E., and Christian, E. L. (2003) Recent insights into the structure and function of the ribonucleoprotein enzyme ribonuclease P, *Curr. Opin. Struct. Biol. 13*, 325−333.
6. Torres-Larios, A., Swinger, K. K., Krasilnikov, A. S., Pan, T., and Mondragon, A. (2005) Crystal structure of the RNA component of bacterial ribonuclease P, *Nature*, 584−587.
7. Kazantsev, A. V., Krivenko, A. A., Harrington, D. J., Holbrook, S. R., Adams, P. D., and Pace, N. R. (2005) Crystal structure of a bacterial ribonuclease P RNA, *Proc. Natl. Acad. Sci. U.S.A.*, 13392−13397.
8. Kazantsev, A. V., Krivenko, A. A., Harrington, D. J., Carter, R. J., Holbrook, S. R., Adams, P. D., and Pace, N. R. (2003) High-resolution structure of RNase P protein from *Thermotoga maritima*, *Proc. Natl. Acad. Sci. U.S.A. 100*, 7497−7502.
9. Stams, T., Niranjanakumari, S., Fierke, C. A., and Christianson, D. W. (1998) Ribonuclease P protein structure: evolutionary origins in the translational apparatus, *Science 280*, 752−755.
10. Tsai, H. Y., Masquida, B., Biswas, R., Westhof, E., and Gopalan, V. (2003) Molecular modeling of the three-dimensional structure of the bacterial RNase P holoenzyme, *J. Mol. Biol. 325*, 661−675.
11. Guerrier-Takada, C., Gardiner, K., Marsh, T., Pace, N., and Altman, S. (1983) The RNA moiety of ribonuclease P is the catalytic subunit of the enzyme, *Cell 35*, 849−857.
12. Loria, A., and Pan, T. (2001) Modular construction for function of a ribonucleoprotein enzyme: the catalytic domain of *Bacillus subtilis* RNase P complexed with *B. subtilis* RNase P protein, *Nucleic Acids Res. 29*, 1892−1897.
13. Pan, T., and Jakacka, M. (1996) Multiple substrate binding sites in the ribozyme from *Bacillus subtilis* RNase P, *EMBO J. 15*, 2249−2255.
14. Nolan, J. M., Burke, D. H., and Pace, N. R. (1993) Circularly permuted tRNAs as specific photoaffinity probes of ribonuclease P RNA structure, *Science 261*, 762−765.
15. Loria, A., and Pan, T. (1997) Recognition of the T stem-loop of a pre-tRNA substrate by the ribozyme from *Bacillus subtilis* ribonuclease P, *Biochemistry 36*, 6317−6325.
16. Chen, J. L., Nolan, J. M., Harris, M. E., and Pace, N. R. (1998) Comparative photocross-linking analysis of the tertiary structures of *Escherichia coli* and *Bacillus subtilis* RNase P RNAs, *EMBO J. 17*, 1515−1525.
17. Oh, B. K., Frank, D. N., and Pace, N. R. (1998) Participation of the 3′-CCA of tRNA in the binding of catalytic Mg^{2+} ions by ribonuclease P, *Biochemistry 37*, 7277−7283.
18. Kufel, J., and Kirsebom, L. A. (1998) The P15-loop of *Escherichia coli* RNase P RNA is an autonomous divalent metal ion binding domain, *RNA 4*, 777−788.
19. Zahler, N. H., Christian, E. L., and Harris, M. E. (2003) Recognition of the 5′ leader of pre-tRNA substrates by the active site of ribonuclease P, *RNA 9*, 734−745.
20. Kole, R., Baer, M. F., Stark, B. C., and Altman, S. (1980) *E. coli* RNAase P has a required RNA component, *Cell 19*, 881−887.
21. Reich, C., Olsen, G. J., Pace, B., and Pace, N. R. (1988) Role of the protein moiety of ribonuclease P, a ribonucleoprotein enzyme, *Science 239*, 178−181.
22. Crary, S. M., Niranjanakumari, S., and Fierke, C. A. (1998) The protein component of *Bacillus subtilis* ribonuclease P increases catalytic efficiency by enhancing interactions with the 5′ leader sequence of pre-$tRNA^{Asp}$, *Biochemistry 37*, 9409−9416.
23. Kurz, J. C., Niranjanakumari, S., and Fierke, C. A. (1998) Protein component of *Bacillus subtilis* RNase P specifically enhances the affinity for precursor-$tRNA^{Asp}$, *Biochemistry 37*, 2393−2400.
24. Kurz, J. C., and Fierke, C. A. (2002) The affinity of magnesium binding sites in the *Bacillus subtilis* RNase P-pre-tRNA complex is enhanced by the protein subunit, *Biochemistry 41*, 9545−9558.
25. Niranjanakumari, S., Stams, T., Crary, S. M., Christianson, D. W., and Fierke, C. A. (1998) Protein component of the ribozyme ribonuclease P alters substrate recognition by directly contacting precursor tRNA, *Proc. Natl. Acad. Sci. U.S.A. 95*, 15212−15217.
26. Niranjanakumari, S., Kurz, J. C., and Fierke, C. A. (1998) Expression, purification and characterization of the recombinant ribonuclease P protein component from *Bacillus subtilis*, *Nucleic Acids Res. 26*, 3090−3096.
27. Behrman, E. J. (2000) An improved synthesis of guanosine 5′-monothiophosphate, *J. Chem. Res. 9*, 446−447.
28. He, B., Rong, M., Lyakhov, D., Gartenstein, H., Diaz, G., Castagna, R., McAllister, W. T., and Durbin, R. K. (1997) Rapid mutagenesis and purification of phage RNA polymerases, *Protein Expression Purif. 9*, 142−151.
29. Rueda, D., and Walter, N. G. (2005) *Methods Mol. Biol.* (in press).
30. Walter, N. G. (2002) *Curr. Protocols Nucleic Acid Chem.*, 11.10.1−11.10.23.
31. Moore, M. J., and Query, C. C. (2000) Joining of RNAs by splinted ligation, *Methods Enzymol. 317*, 109−123.
32. Crary, S. M. (1999) Investigation into the mechanism of the bacterial RNase P: The role of the protein component and the identification of direct metal ligands, Thesis in Biochemistry, Duke University, Durham, NC.

33. Walter, N. G. (2001) Structural dynamics of catalytic RNA highlighted by fluorescence resonance energy transfer, *Methods 25*, 19−30.
34. Rueda, D., Wick, K., McDowell, S. E., and Walter, N. G. (2003) Diffusely bound Mg^{2+} ions slightly reorient stems I and II of the hammerhead ribozyme to increase the probability of formation of the catalytic core, *Biochemistry 42*, 9924−9936.
35. Walter, N. G., Burke, J. M., and Millar, D. P. (1999) Stability of hairpin ribozyme tertiary structure is governed by the interdomain junction, *Nat. Struct. Biol. 6*, 544−549.
36. Cunliffe, J. M., Liu, Z., Pawliszyn, J., and Kennedy, R. T. (2004) Use of a native affinity ligand for the detection of G proteins by capillary isoelectric focusing with laser-induced fluorescence detection, *Electrophoresis 25*, 2319−2325.
37. Lohman, T. M., and Mascotti, D. P. (1992) Nonspecific ligand-DNA equilibrium binding parameters determined by fluorescence methods, *Methods Enzymol. 212*, 424−458.
38. Fang, X. W., Yang, X. J., Littrell, K., Niranjanakumari, S., Thiyagarajan, P., Fierke, C. A., Sosnick, T. R., and Pan, T. (2001)- The *Bacillus subtilis* RNase P holoenzyme contains two RNase P RNA and two RNase P protein subunits, *RNA 7*, 233−241.
39. Barrera, A., Fang, X., Jacob, J., Casey, E., Thiyagarajan, P., and Pan, T. (2002) Dimeric and monomeric *Bacillus subtilis* RNase P holoenzyme in the absence and presence of pre-tRNA substrates, *Biochemistry 41*, 12986−12994.
40. DeLano, W. (2002) PyMOL, DeLano Scientific, San Carlos, CA.
41. Lakowicz, J. R. (1999) *Principles of Fluorescence Spectroscopy*, 2nd ed., Kluwer Academic, Norwell, MA.
42. Harris, D. A., Rueda, D., and Walter, N. G. (2002) Local conformational changes in the catalytic core of the trans-acting hepatitis delta virus ribozyme accompany catalysis, *Biochemistry 41*, 12051−12061.
43. Glass, J., and Wertz, G. W. (1980) Different base per unit length ratios exist in single-stranded RNA and single-stranded DNA, *Nucleic Acids Res. 8*, 5739−5751.
44. Saenger, W. (1984) *Principles of Nucleic Acid Structure*, Springer-Verlag, New York.
45. Seol, Y., Skinner, G. M., and Visscher, K. (2004) Elastic properties of a single-stranded charged homopolymeric ribonucleotide, *Phys. Rev. Lett. 93*, 118102.
46. Walter, N. G., and Burke, J. M. (1997) Real-time monitoring of hairpin ribozyme kinetics through base-specific quenching of fluorescein-labeled substrates, *RNA 3*, 392−404.
47. Guerrier-Takada, C., and Altman, S. (1984) Catalytic activity of an RNA molecule prepared by transcription in vitro, *Science 223*, 285−286.
48. Kim, J. J., Kilani, A. F., Zhan, X., Altman, S., and Liu, F. (1997) The protein cofactor allows the sequence of an RNase P ribozyme to diversify by maintaining the catalytically active structure of the enzyme, *RNA 3*, 613−623.
49. Westhof, E., Wesolowski, D., and Altman, S. (1996) Mapping in three dimensions of regions in a catalytic RNA protected from attack by an Fe(II)-EDTA reagent, *J. Mol. Biol. 258*, 600−613.
50. Buck, A. H., Dalby, A. B., Poole, A. W., Kazantsev, A. V., and Pace, N. R. (2005) Protein activation of a ribozyme: the role of bacterial RNase P protein, *EMBO J.*, 3360−3368.
51. Gopalan, V., Baxevanis, A. D., Landsman, D., and Altman, S. (1997) Analysis of the functional role of conserved residues in the protein subunit of ribonuclease P from *Escherichia coli*, *J. Mol. Biol. 267*, 818−829.
52. Biswas, R., Ledman, D. W., Fox, R. O., Altman, S., and Gopalan, V. (2000) Mapping RNA-protein interactions in ribonuclease P from *Escherichia coli* using disulfide-linked EDTA-Fe, *J. Mol. Biol. 296*, 19−31.
53. Heide, C., Busch, S., Feltens, R., and Hartmann, R. K. (2001) Distinct modes of mature and precursor tRNA binding to *Escherichia coli* RNase P RNA revealed by NAIM analyses, *RNA 7*, 553−564.
54. Kaye, N. M., Christian, E. L., and Harris, M. E. (2002) NAIM and site-specific functional group modification analysis of RNase P RNA: magnesium dependent structure within the conserved P1−P4 multihelix junction contributes to catalysis, *Biochemistry 41*, 4533−4545.
55. Buck, A. H., Kazantsev, A. V., Dalby, A. B., and Pace, N. R. (2005) Structural perspective on the activation of RNase P RNA by protein, *Nat. Struct. Mol. Biol.* (in press).
56. Oubridge, C., Ito, N., Evans, P. R., Teo, C. H., and Nagai, K. (1994) Crystal structure at 1.92 Å resolution of the RNA-binding domain of the U1A spliceosomal protein complexed with an RNA hairpin, *Nature 372*, 432−438.
57. Mattaj, I. W., and Nagai, K. (1995) Recruiting proteins to the RNA world, *Nat. Struct. Biol. 2*, 518−522.
58. Niranjanakumari, S., Day-Storms, J. J., Venters, R. A., and Fierke, C. A. (2005) unpublished results.

BI0519093